communications materials

A Nature Portfolio journal

Article

https://doi.org/10.1038/s43246-026-01079-z

Intrinsically colored artificial silk fibers made from mini-spidroin fusion proteins

Tomas Bohn Pessatti[1,5], Benjamin Schmuck[1,5], Gabriele Greco[1], Sarah Stadlmayr[2], Elin Karlsson[1], Bryan Gross[1], Axel Leppert[3], Michael Landreh[3,4] & Anna Rising[1,2]

Spider silk is an extraordinary natural material that combines strength, extensibility, and toughness in a lightweight, protein-based fiber. While the recombinant production of spidroins has advanced, the creation of silk fibers with additional intrinsic functionalities, such as color, remains a major challenge. Here, we report the rational design, expression, and spinning of intrinsically red-colored artificial silk fibers. A mini-spidroin variant was engineered as a fusion with the red fluorescent protein mCherry, expressed at high yields (20 g/L) in *E. coli* fed-batch fermentations, and purified under native conditions. Although the presence of the mCherry globular domain reduced spinnability when used alone, blending with wild-type mini-spidroins enabled continuous wet spinning into robust, fluorescent fibers. Our biomimetic spinning approach preserved the correct folding of the mCherry domain within the fiber, resulting in stable red coloration and fluorescence, while maintaining mechanical properties comparable to those of other recombinant silks. This work establishes a scalable, sustainable strategy for fabricating colored bio-based fibers, opening avenues for environmentally friendly textiles and functional biomaterials that may reduce reliance on synthetic and chemically dyed fibers.

Spider silk has long been recognized as one of nature's toughest and most resilient fibers, combining high tensile strength with exceptional extensibility[1,2]. These properties have made it a source of inspiration for developing new high-performance materials[3–6]. Recombinant mini-spidroins[7], simplified versions of native spider silk proteins, have enabled progress toward scalable silk production[8]. Despite this, the commercialization and market penetration of artificial spider silk materials have remained slow[3,4]. Several factors may explain the limited impact of artificial spider silk in industry, including a relatively high production cost[3], but also that the unique features and potential of artificial spider silk remain unutilized. Since artificial spider silk is a protein-based material, it can be engineered to incorporate intrinsic functionalities. There are several examples in the scientific literature where functionalization was introduced into silk-based materials post-assembly (after the material was formed), including site-specific functionalization with antibody binding or antimicrobial properties using enzymes[9], or functionalization of artificial spider silk with green fluorescent protein (GFP) using biomolecular click chemistry[10]. However, a simpler and more straightforward way of making functionalized fibers would be to express fusion proteins that can assemble into fibers with intact function of the bioactive fusion partner. A major problem for achieving this would be that most published wet-spinning protocols rely on the use of harsh denaturing conditions[11–14], which leads to loss of the bioactivity of the fusion partner.

One potentially useful application of bioactive fibers would be to equip them with color. Dye synthesis for textile applications relies on fossil-based feedstock[15,16] and many dyes contribute to significant environmental harm and pose various health risks[17]. In addition to the dyes' toxicity, the pre-treatment process alone requires 200 L of fresh water per kg of fabric[18], and massive amounts of contaminated water are released into the environment[19]. Even though new eco-friendly technologies have been developed, their implementation in the textile dyeing process remains negligible[20], since alternative dyes cannot yet compete in terms of availability, variety of colors, and price[21].

For making intrinsically colored protein-based fibers, fluorescent proteins, such as GFP[10], or colored proteins[22] could be used, provided that the spinning process is void of denaturing conditions. The recently developed all-aqueous biomimetic spinning method for making artificial spider silk[7] opens up a unique possibility to design recombinant fusion proteins

[1]Department of Animal Biosciences, Swedish University of Agricultural Sciences, Uppsala, Box 7023, 75007, Sweden. [2]Department of Medicine Huddinge, Karolinska Institutet, NEO, Huddinge, 14183, Sweden. [3]Department for Cell and Molecular Biology, Uppsala University, Uppsala, 75124, Sweden. [4]Department of Microbiology, Tumor and Cell Biology, Karolinska Institutet, Solna, 171 65, Sweden. [5]These authors contributed equally: Tomas Bohn Pessatti, Benjamin Schmuck. e-mail: anna.rising@slu.se

consisting of mini-spidroins covalently linked to colored proteins[23,24]. Such a bio-based strategy to produce intrinsically colored fibers at the protein level could eliminate the need for post-spinning dyeing, offering a more sustainable alternative. Beyond textiles, colored and fluorescent silk fibers could enable new biomedical applications, such as tracking material integration in vivo or designing smart materials with built-in optical signals.

Here, we demonstrate a protein engineering approach that paves the way towards this goal by generating a fluorescent mini-spidroin that can be produced at high yields and spun into functionally intact composite fibers with robust mechanical properties. Thus, this work establishes a scalable, all-aqueous route to producing bio-based, bioactive fibers, highlighting their potential as sustainable alternatives to conventional fibers.

Results and discussion

A_3I-A-mCherry can be expressed and purified under native conditions

Building on our previously described method for producing mini-spidroins under native conditions[8,25], and our biomimetic and all-aqueous spinning process[7,26], we explored whether fluorescent protein fusions can be used to generate intrinsically colored silk fibers. We hypothesized that the high expression yields obtained for these mini-spidroins, combined with the mild processing conditions, would enable the development of fibers with colors derived from folded globular proteins. To test this, a fusion protein consisting of the mini-spidroin $(A_3I)_3$-$(A)_{14}$[25] fused to the red-fluorescent protein mCherry [27] (Fig. 1) was designed, where the C-terminal mCherry moiety was separated from the CT domain by a double $(GS)_8$ linker (see Supplementary information for all sequences). Hereafter, the fusion protein is referred to as A_3I-A-mCherry. Initial tests showed that A_3I-A-mCherry could be over-expressed in *E. coli* shake-flask cultures and had the expected molecular weight of approximately 62 kDa (Fig. S1). Following lysis in 20 mM Tris (pH 8.0), the fusion protein could be purified from the soluble fraction using affinity chromatography (Fig. S1).

Real-world applications of colored fibers depend on their scalable production. We therefore set out to scale up the fermentation process in a fed-batch bioreactor cultivation using previously published protocols (Fig. 2A)[8]. From a 7.63 L culture, 2353 g of wet cell pellet was obtained (Fig. S2), which corresponds to 308 g wet cell mass per L of culture. The amount of A_3I-A-mCherry expressed was estimated with SDS-PAGE to 20 g of protein per liter of the bioreactor culture (Fig. S3), or 66 mg of protein per gram of wet-cell pellet. SDS-PAGE of the soluble and insoluble fractions after lysis indicated that a majority of the target protein was soluble after cell lysis (Fig. 2B). After separation of the soluble fraction, affinity chromatography purification under native conditions yielded 10 g/L of culture, or 35 mg/g of wet cell pellet (Fig. 2B and Fig. S2D). This yield is in line with what has been estimated as economically feasible for making high-end textile fibers[28]. Mass spectrometry confirmed the expected protein mass of 62.05 kDa, and together with mass photometry measurements, indicated that A_3I-A-mCherry exists predominantly as 124.1 kDa dimers in solution, consistent with the constitutive dimer conformation of the C-terminal domain[7,29,30]. A smaller fraction of higher-molecular-weight oligomers was also observed (Fig. 2C, D and Figure S4). Interestingly, the fusion protein appeared to be equally soluble in 20 mM Tris (pH 8) as the $(A_3I)_3$-$(A)_{14}$ and could be concentrated to about 300 mg/mL without visible aggregation. A strong burgundy color and red fluorescence under UV light indicated that the mCherry fusion partner was functional, and therefore correctly folded (Fig. 3A).

Bioactive fluorescent fibers can be wet-spun with retained mechanical properties

After establishing that the A_3I-A-mCherry could be produced and purified under native conditions, we next evaluated its ability to undergo fiber formation. To this end, concentrated protein solutions were subjected to wet spinning to assess spinnability, fiber stability, and retention of fluorescence. The wet-spinning methodology described in this work is excellent for introducing intrinsic functionality to wet-spun artificial spider silk, as it is all-aqueous, completely void of high temperatures, denaturing agents, and harsh solvents, and polymerization into fibers is achieved by a mild pH drop from pH 8 in the spinning feedstock to pH 5 in the fiber collection bath[7,8,26]. In a first attempt, A_3I-A-mCherry could not be spun into continuous fibers: the fibers were too brittle to handle and could not be continuously collected by mechanical reeling. Considering that the fusion partner (mCherry) is almost the same size as the mini-spidroin moiety, it is not surprising that the presence of this large folded globular protein negatively affects the polymerization process.

To overcome the poor spinnability of pure A_3I-A-mCherry, the fusion protein was mixed with $(A_3I)_3$-$(A)_{14}$. This approach effectively solved the spinning limitations, as mixtures containing 12.5, 25, and 50% (w/w) of A_3I-A-mCherry were readily wet-spun into stable fibers. These fibers exhibited sufficient integrity to enable continuous collection on a rotating take-up wheel. Notably, the wet-spun fibers retained a burgundy-like color under white light after spinning and exhibited red fluorescence under UV illumination (Fig. 3B and Fig. S5), indicating that a substantial fraction of the mCherry moiety remained intact. Precise quantification of the fraction of correctly folded mCherry is challenging due to concentration changes during the fiber drying, the influence of water content, fiber opacity, and structural alterations induced by the fiber dissolution protocols. Instead, to get an indication of how well the mCherry tolerates the spinning conditions, we exposed the A_3I-A-mCherry spinning dope to a low-pH acetate buffer and subsequent drying. No reduction in fluorescence was observed (Fig. S6), which indicates that mCherry can maintain its fold during the spinning process. As expected, we found a positive correlation between mCherry concentration in the spinning dope and fluorescence in the fiber (Fig. 3C and Fig. S6). Furthermore, structural characterization of the fibers containing mCherry and pure $(A_3I)_3$-$(A)_{14}$ by attenuated total reflectance Fourier-Transform Infrared (ATR-FTIR) spectroscopy revealed that the fibers containing mCherry, had an increased absorbance around 1630 cm^{-1}, which is in line with the native beta barrel fold of mCherry (Fig. S7). Collectively, these results suggest that a large fraction of the mCherry moieties are folded and functional, also after spinning.

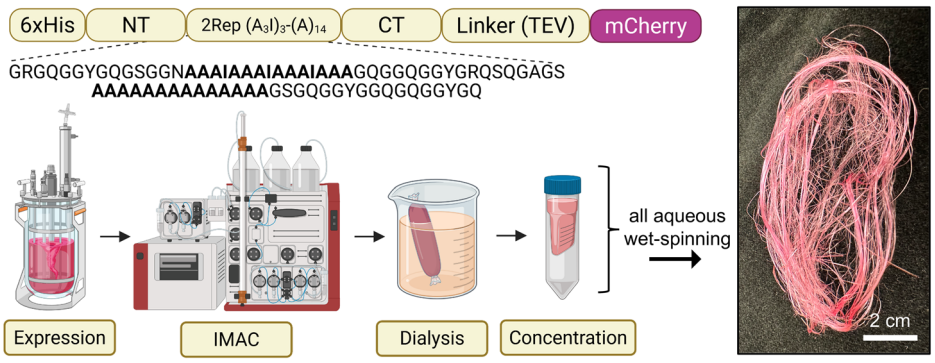

Fig. 1 | The red fluorescent protein mCherry was fused to the mini-spidroin $(A_3I)_3$-$(A)_{14}$. The full sequence of the fusion protein is shown in the Supplementary Information. The fusion protein was expressed using *E. coli* in a bioreactor, purified with chromatography (IMAC), and wet-spun into red-fluorescent fibers using an all-aqueous spinning setup. The picture of the fiber bundle shown on the right was taken ~1 week after spinning. The illustration was created with Biorender.com.

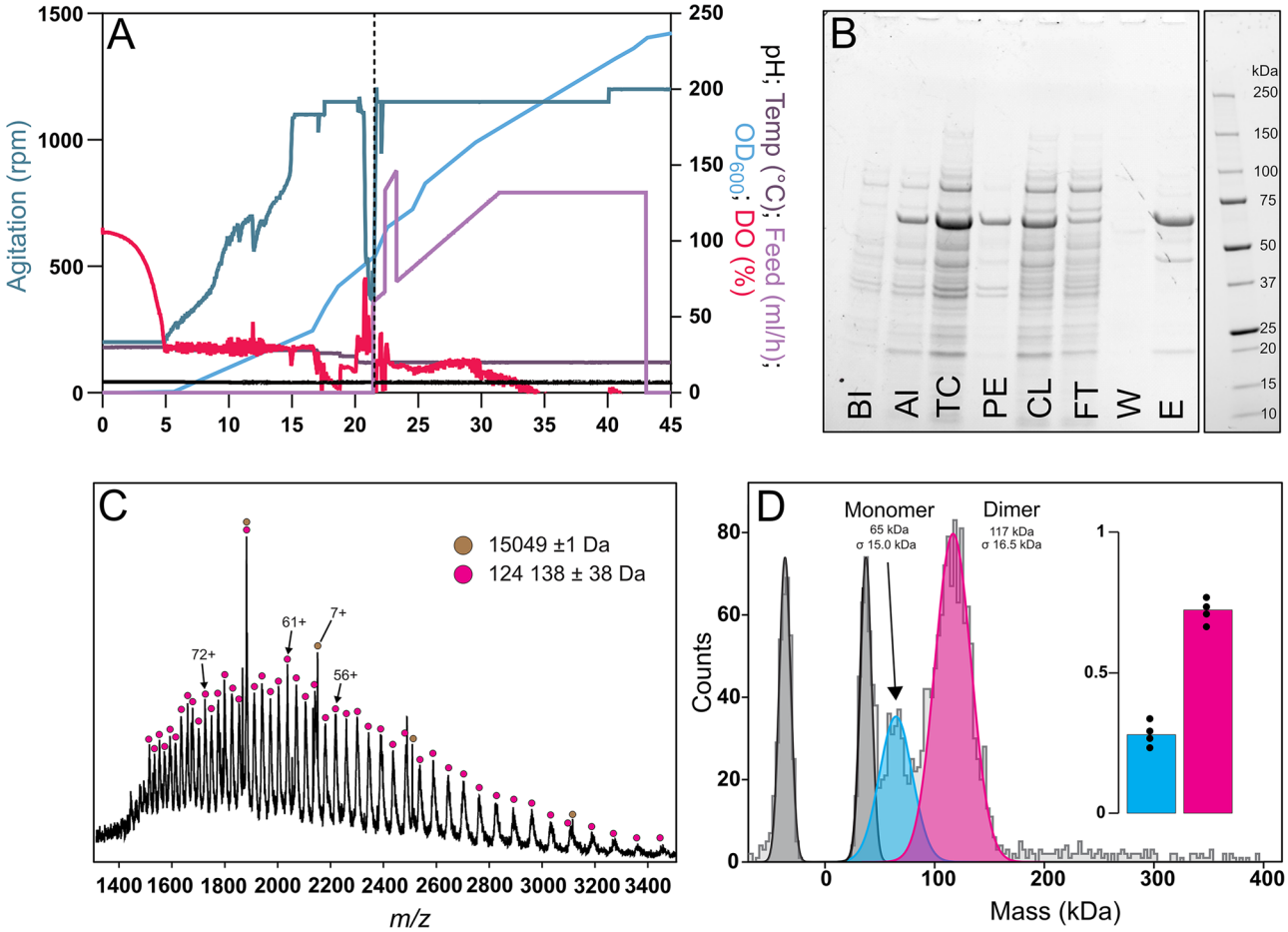

Fig. 2 | Fed-batch expression and IMAC purification of A_3I-A-mCherry yield a soluble dimeric fusion protein. A Cultivation profile of a 45-hour fed-batch *E. coli* culture. Indicated parameters include agitation (impeller speed, in rpm); pH; temperature (°C); feed medium addition (rate of feed pump, in mL/h); OD_{600}, optical density (absorbance at 600 nm); DO, dissolved oxygen (%). **B** SDS-PAGE of cell culture before (BI) and after induction (AI). The sample BI was taken minutes before the protein expression was induced (21.5 h after inoculation) and is indicated by a dashed line in panel **A**. The sample AI was obtained 23.4 h after induction, just before the biomass was harvested by centrifugation. The gel also includes fractions from the purification: Total cell lysate (TC); Pellet after centrifugation (PE); Supernatant after centrifugation – the clarified lysate (CL); IMAC flow through (FT); Wash (W); and eluate (E). The additional bands observed in the SDS-PAGE in lane E, migrating below A_3I-A-mCherry, likely correspond to intramolecular cleavage products of mCherry formed during the denaturation process, as previously reported[41]. An estimation of the A_3I-A-mCherry concentration in the AI sample is shown in Figure S3. **C** Mass spectrum (m/z) with indicated charge states and the calculated mass matching the molecular weight of a dimer (Da). **D** Mass photometry histogram indicating the mass distribution in a sample of A_3I-A-mCherry ($n = 4$), where blue shows the monomer peak, and magenta the dimer peak. The inserted histogram shows the average ratio of monomer vs. dimers. The black dots indicate the results from individual measurements. The grey peaks in the positive and negative molecular weight range indicate buffer noise. Mass photometry histogram of bovine serum albumin (BSA), the calibrant, is shown in Fig. S4.

An important factor to consider for practical applications of the functional fibers is the stability of the immobilized fusion moiety over time. To assess this, a fluorescence microscope was used to measure fluorescence immediately after spinning, and 1 day, 3 days, and 7 days after spinning for the 50% A_3I-A-mCherry fibers. Interestingly, fluorescence remained stable throughout the entire measurement period (Fig. 3D and Fig. S6).

The morphology of the fibers was assessed with confocal and brightfield microscopy, which revealed a longitudinal groove along the axis of the fibers, which is a feature commonly observed for wet-spun fibers[31]. To assess the fibers' mechanical properties, they were subjected to standardized tensile tests[26,31,32]. A trend towards reduced strength with increasing amounts of mCherry, was observed, while the strain was simultaneously increased (Fig. 3E). However, statistically significant differences ($p < 0.05$) were only observed when comparing the fibers in the two extremes: $(A_3I)_3$-$(A)_{14}$ only, and 50% (w/w) of A_3I-A-mCherry. Notably, the A_3I-A-mCherry fibers displayed tensile strengths between 67 and 115 MPa, which is within the same range reported for other artificial silk fibers spun using aqueous buffers and a drop in pH from 8 to 5[25,26,32,33]. To our surprise, there was no significant difference in the toughness modulus between the different fibers, including those made from pure $(A_3I)_3$-$(A)_{14}$.

Wet-spinning without the need for post-processing represents the next stage in the evolution of functionalized artificial silk-based materials[10,34,35]. Our approach serves as a proof of concept that not only simplifies the production but also preserves the functionality of the incorporated functional moiety during a continuous spinning process, thereby supporting scalability. To enable commercial implementation, this class of materials should next be evaluated against standardized performance criteria by the textile industry.

Conclusion

In this study, we demonstrate the fabrication of continuous, intrinsically colored silk fibers through direct protein engineering and aqueous wet spinning. By fusing a mini-spidroin with mCherry and co-spinning it with

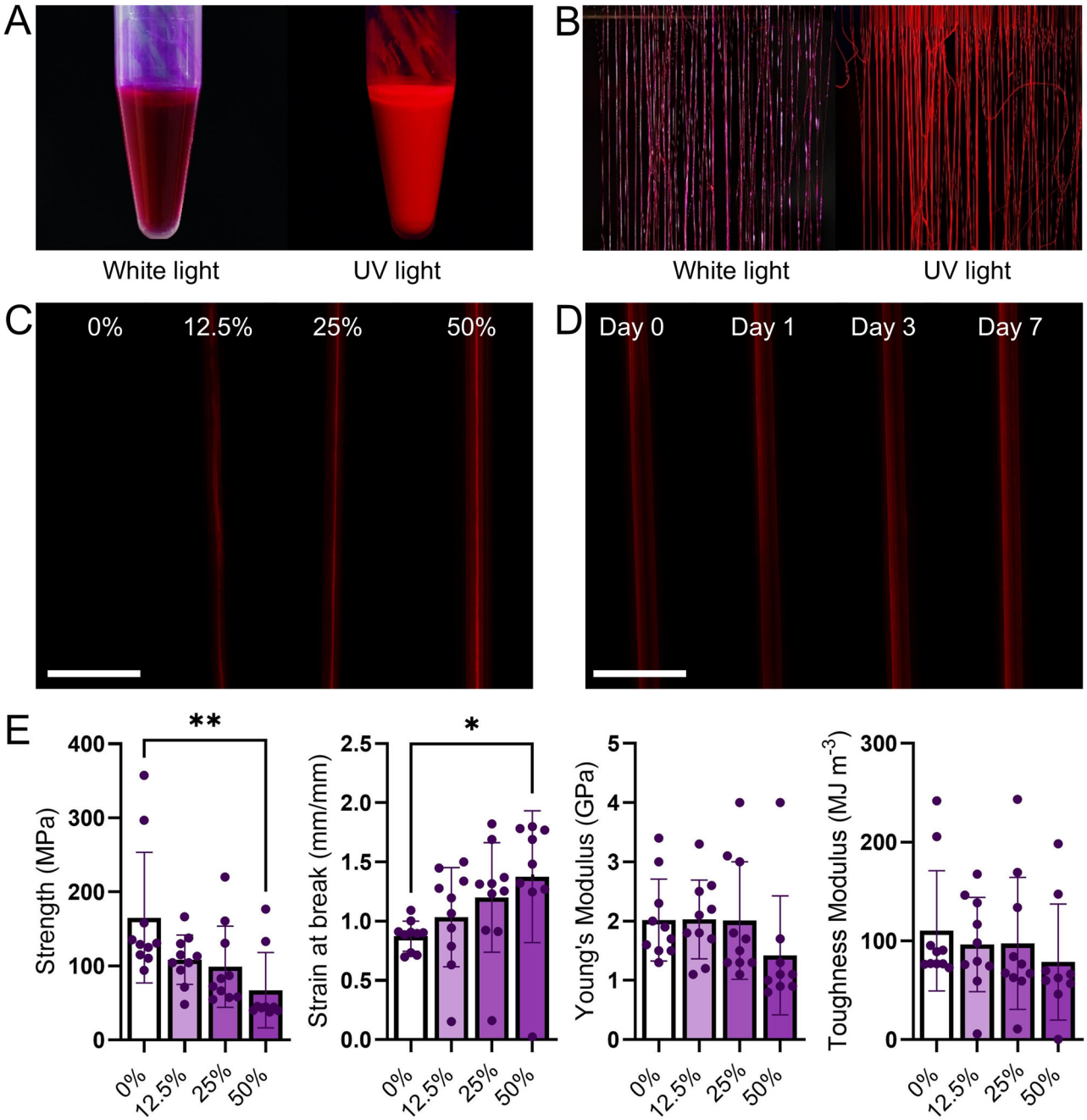

Fig. 3 | A_3I-A-mCherry mixed with $(A_3I)_3$-$(A)_{14}$ can be wet-spun into fluorescent fibers with retained mechanical properties using an all-aqueous and biomimetic spinning method. A 100% (w/w) A_3I-A-mCherry at 300 mg/ml under white (left) and UV light (right). **B** 50% (w/w) A_3I-A-mCherry fibers under white light (left) and UV light (right). **C** Representative fluorescent images showing fibers with increasing content in % (w/w) of A_3I-A-mCherry, as indicated at the top of each fiber. The scale bar indicates 170 µm. **D** Representative fluorescent images showing fibers with an A_3I-A-mCherry content of 50%. The images were taken immediately, as well as one day, three days, and seven days after spinning. The scale bar indicates 170 µm. Representative brightfield images and quantified fluorescence intensities for **C** and **D** are shown in Fig. S6. **E** Mechanical properties of fibers spun from different mixtures of A_3I-A-mCherry and $(A_3I)_3$-$(A)_{14}$. The fraction of A_3I-A-mCherry is given as % (w/w) in the dry fiber. For each fiber type, 10 fibers were tensile tested. The staples indicated the average, and the whiskers ± one standard deviation. Not significant for $p \geq 0.05$; $^*p < 0.05$; $^{**}p < 0.01$. Additional pictures of the as-spun fibers, all diameter values and representative stress-strain curves are shown in Fig. S5.

non-fluorescent constructs, we could continuously spin fibers that combine mechanical performance with stable red coloration and fluorescence. Due to the mild spinning conditions, this approach provides a scalable and environmentally sustainable route to functional silk-based materials. Beyond serving as a proof of concept for bioactive and fluorescent silks, our strategy highlights the potential of engineered spidroins as a new class of bio-based fibers that could one day complement or replace petroleum-derived synthetic fibers in textiles and other advanced material applications.

Methods

Fusion protein design and cloning

The $(A_3I)_3$-$(A)_{14}$ was fused to mCherry (GeneBank: accession number AY678264.1) on the C-terminal end using a linker containing a TEV-cleavage site (full sequence in Supplementary Information). Both $(A_3I)_3$-$(A)_{14}$ and A_3I-A-mCherry were fused to an hexahistidine (His_6) -tag on the N-terminal end. For the expression of $(A_3I)_3$-$(A)_{14}$, the same plasmid as described by Arndt and coworkers was used[25]. The mCherry tag was codon-

optimized, synthesized by GeneScript, and cloned into the vector containing $(A_3I)_3$-$(A)_{14}$ using the restriction enzymes HindIII and AscI. After ligation, the *E. coli* Nova Blue were transformed by heat shock and plated on an LB-agar plate containing 70 μg/mL Kanamycin, and incubated overnight at 37 °C. Positive colonies were picked, and a miniprep was prepared using the QIAprep® Spin Miniprep Kit (QIAGEN), according to the manufacturer's instructions. The purified plasmids were sequenced before transformation into chemically competent *E. coli* BL21 (DE3).

Fusion protein expression and purification

The $(A_3I)_3$-$(A)_{14}$ and A_3I-A-mCherry were expressed as previously described, using a bioreactor cultivation[8,25]. Briefly, we followed a protocol originally developed by da Silva and coworkers[36]. Using an Eppendorf BioFlo 120 equipped with a 13 L single-walled glass vessel, 5 L of autoclaved medium was prepared by autoclaving the main components in the reaction vessel, followed by separate addition of sterile stock solutions of filtered glucose (700 g/l), trace metal solution (50×), and $MgSO_4 \cdot 7H_2O$ (500 g/L). All components and their final concentrations in the batch medium are listed in Table S1. In addition, antifoam 204 (final concentration 0.01%) and kanamycin (final concentration 30 μg/mL) were added before the medium was inoculated with a day culture (LB medium) of *E. coli*, to reach a final OD_{600} of 0.1. During the batch phase, the bacteria were grown at 28 °C, with a constant pH of 7.0 maintained by adjusting the pH with either 3 M H_3PO_4 or 25% NH_3. The dissolved oxygen (DO) level was set to 30% and automatically adjusted by the BioCommand software (version 6.03, Eppendorf), by first increasing the air flow from 2 L/min to 20 L/min and then by increasing the stirring speed from 200 rpm to a maximum of 1000 rpm. Once the culture reached an OD_{600} of ~70, the temperature was decreased to 20 °C. Afterward, protein expression was induced by adding IPTG to a final concentration of 150 μM (21.5 h after inoculation). The feeding of the culture was initiated once a spike in DO levels was observed, indicating the depletion of the carbon source in the batch medium. During the feeding phase, consisting of a linear increase for 10 h (58-143 mL/h), followed by constant feeding (143 mL/h) for an additional 10 h, up to 2.5 L of feed was added, containing 60% (w/v) Glycerol. All components and their final concentrations in the feed medium are listed in Table S1.

23.5 h after induction, the biomass was harvested by centrifugation at 4000 × g for 20 min, and 4 °C, the supernatant (SN) was discarded. The cell pellet was weighed and resuspended by adding an equal volume of Tris buffer (20 mM Tris-HCl, pH 8), followed by gentle swirling in an incubator at 10 °C and 100 rpm. The cell pellet resuspension was stored at −20 °C.

For purification, we followed a previously published protocol using immobilized metal affinity chromatography (IMAC), with minor adjustments[8]. The cell pellet resuspension was placed in ice-cold Tris buffer to reach a final ratio of wet cell pellet to buffer of 1:10 and thawed by stirring. The resuspended cells were lysed using a CF1 cell disruptor (Constant Systems) at 4 °C. Then, the lysate was centrifuged at 17,500 × *g* for 1 h, also at 4 °C. The pellet was discarded, but the SN was directly loaded onto a HiScale 50/40 (Cytiva) filled with 700 mL Capto Chelating (Cytiva), charged with Ni^{2+}, at up to 80 mL/min using an Äkta Avant (Cytiva) in the cold room at 6 °C. The column was washed with Tris-buffer, containing 2 mM imidazole, until the mAU at 280 nm reached below 150. Then, the His_6-tagged proteins were eluted with Tris buffer containing 200 mM imidazole. From one binding and elution cycle (90 min), around 9 g of target protein was purified. The eluate was dialyzed against a Tris buffer, with several buffer exchanges to achieve a final dilution factor of 280,000, using a Spectra/Por dialysis membrane (Spectrum Labs) with a 6–8 kDa molecular weight cutoff. After dialysis, the protein concentration and yield of the purification were determined by measuring the absorbance at 280 nm with a spectrophotometer in 20 mM TrisHCl buffer. To calculate the concentration, we used the protein-specific extinction coefficient computed with the Protparam tool available on the Expasy server[37]. The expression and purification were then analyzed using SDS-PAGE. Samples taken directly from the bioreactor culture were diluted 40× (before and after induction) in 8 M Urea in Tris buffer. Total cell (after lysis), Pellet (insoluble fraction), SN (soluble fraction), and FT (IMAC flow through) were diluted 10×, also using 8 M Urea in Tris buffer. The IMAC wash fraction was not diluted, and the eluate was diluted 5×, also using 8 M Urea in Tris buffer. Then, the diluted samples were mixed with an equal amount of 2× Laemmli + β-mercaptoethanol buffer, heated to 95 °C for 5 min, followed by centrifugation. 7 μl of each sample was loaded onto a 15-well Mini-PROTEAN TGX Stain-Free Precast Gel 4–20% (Bio-Rad). The gel was imaged using a ChemiDoc Touch (Bio-Rad). After confirming the purity of the proteins, all purified proteins were stored at −20 °C.

Spinning dope preparation

Purified $(A_3I)_3$-$(A)_{14}$ and A_3I-A-mCherry was filtered through 0.2 μm and concentrated to 300 mg/mL using a 500 mL stirred cell device (Merck Millipore) equipped with a 10 kDa molecular weight cutoff membrane, at 6 °C, and nitrogen up to 4 bars. To obtain the final spinning dope containing 0%, 12.5%, 25%, and 50% of A_3I-A-mCherry in $(A_3I)_3$-$(A)_{14}$, both were mixed from solutions having an equal concentration of 300 mg/mL. Due to the high viscosity of the spinning dope, a homogeneous mixture was obtained by stirring with a spatula, followed by brief centrifugation at 1000 × *g*, and repeating the process 4–5 times. The spinning dope was then transferred into a 1 mL syringe with a Luer lock (BD) and then stored at −20 °C.

Mass photometry

Mass photometry experiments were performed on a TwoMP instrument (Refeyn) in standard measurement mode with regular image size. A_3I-A-mCherry (2.8 mM) was diluted to a final concentration of 8 nM in 20 mM Tris (pH 8). 2 nM Bovine serum albumin (66 kDa and 132 kDa) from Sigma Aldrich (A7030) in 20 mM Tris (pH 8) was used as a mass calibrant. Four independent measurements were acquired, each for 1 min (3000 frames), using the AcquireMP software (version 2024 R1.1). Data were processed in DiscoverMP (Refeyn), where histograms were generated and fitted with a Gaussian function. Monomer/dimer ratios were determined from the integrated counts under the respective peaks.

Native mass spectrometry

A_3I-A-mCherry (2.8 mM) was diluted into 50 mM ammonium acetate, pH 8, to a final concentration of 10 μM. Samples were loaded into nESI capillaries (Thermo Fisher Scientific). Mass spectra were recorded in positive ionization mode on a Waters Synapt G1 traveling-wave IM mass spectrometer (MS Vision). The capillary voltage was maintained at 1.5 kV, and the sample cone voltage was 100 V. The source temperature was 30 °C. The trap and transfer collision energies were 20 V. The trap gas was argon at a flow rate of 1.5 mL/min, the IMS gas was nitrogen at a flow rate of 18.5 mL/min. Spectra were analyzed using MassLynx 4.1 (Waters).

All-aqueous spinning

The spinning dope at 300 mg/mL was extruded at room temperature through an A-150250000SA-B278 nozzle (Tecdia) into an 80 cm long coagulation bath containing a 0.75 M acetate buffer (pH 5), where the fiber was immediately formed. The tip of the nozzle was tapered and had an orifice diameter of 150 μm. The extrusion rate of the spinning dope was 45 μl/min. The fiber was carefully picked up and placed onto a rotating wheel, where it was transferred into a second bath also containing 0.75 M acetate buffer (pH 5). At the end of the second bath, the fiber was continuously collected in air at a rate of up to 35 cm/s. Fibers were stored in a drying cabinet with a relative humidity (RH) of less than 20%.

Brightfield and fluorescence imaging

All spun fibers were visualized on an Echo Revolve R4 (Discover Echo) hybrid microscope operated in upright mode at 10× magnification (UPLFLN 10×/0.3 NA, Olympus Life Science).

Brightfield microscopy was performed to assess fiber morphology. Brightfield images were acquired using LED-transmitted illumination with

the light intensity set to 100% and the camera operating in high-gain mode to ensure sufficient contrast across the full fiber thickness. Acquisition parameters were kept constant for all samples to allow qualitative comparison between fiber populations and concentrations.

Fluorescence images were acquired using an LED light intensity of 15% and an exposure time of 5 ms for all conditions. Multichannel Z-stack images were collected using the TxRED fluorescence channel to capture the full thickness of the fibers and were reconstructed using Extended Depth of Field (EDF) mode to generate a single in-focus image per fiber.

Fluorescence images were analysed using ImageJ (version 1.54p, National Institutes of Health)[38]. EDF images were converted to 16-bit, and the spatial scale was defined at 0.36 µm/pixel. The normalized Corrected Total Fluorescence per unit area (CTF/µm^2) was calculated following the equation:

$$CTF = \frac{\left[Intensity\ signal - Mean_{Background}\right]}{Area_{ROI}}$$

These values were used for quantitative comparison of fibers made from spinning dope containing 0% 12.5%, 25%, and 50% A_3I-A-mCherry concentration. In addition, mCherry stability over time was assessed using fibers containing 50% A_3I-A-mCherry, which were analyzed immediately after spinning (within 45 min) and after 1, 3, and 7 days. For each fiber type, three independent fibers were imaged three times at random positions (= 9 pictures per type). In addition, for each picture, three regions of interest (ROIs) were randomly defined along the fiber to determine the intensity signal (i.e., $n = 27$ ROIs for each concentration), while the background was determined from 0% fiber.

Attenuated total reflection Fourier-transformed infrared spectroscopy (ATR-FTIR)

ATR-FTIR analysis was carried out on individual fibers using an Invenio S spectrometer (Bruker) equipped with a Platinum-ATR accessory and an LN-MCT detector, following a protocol adapted from Greco et al.[39]. Both the ATR unit and the spectrometer optical path were continuously purged with dry, filtered N_2 during the experiments. Fibers were carefully positioned on the ATR crystal, either parallel or perpendicular to the incident IR beam, and gently pressed into contact using the piston. The applied pressure was minimized to avoid fiber damage or pressure-induced spectral artifacts[40]. FTIR measurements were performed using an aperture of 1 mm, a scanner velocity of 60 kHz, and an absorbance range of 4000–750 cm^{-1}. Spectra were collected at a resolution of 2 cm^{-1} with 300 scans accumulated per sample. The spectra obtained for each fiber type were background-subtracted and averaged with Bruker OPUS software v 9.0. The spectra were normalized with respect to the highest peak with F. Menges's "Spectragryph – optical spectroscopy software". No smoothing was applied.

Confocal microscopy

Fluorescence intensity was recorded of fresh 50% A_3I-A-mCherry spinning dope, as well as dope that was dried, dope submerged in acetate buffer (pH 5), and dope submerged in acetate buffer (pH 5) for 30 s with subsequent drying (60 min) in µ-slide 8 well (ibidi). Imaging was performed on a NIKON AxR confocal microscope equipped with 20 × objective (CFI Plan Apochromat Lambda D, NIKON) using the NIS-Elements ER software (version 6.10.02, NIKON) with an excitation of 561 nm and an emission range of 592–721 nm. All images were acquired using a galvano scanner with an averaging of 2, a dwell time of 1.2, laser intensity set to 0.1, and a gain of 28.9. Samples were recorded as z-stacks using the optimal step size (0.46 µm) and Nyquist resolution (0.144 µm). For the dope samples, the plane of highest fluorescence intensity was set as the center, and a symmetric z-stack of 70 µm for one position was recorded. The image with the highest fluorescence intensity was selected for evaluation of fluorescence intensity using ImageJ (version 1.54p, National Institutes of Health)[38] and corrected for the respective background. The pixel size was set to 0.14 µm, and subsequent steps were conducted as outlined in the Brightfield and Fluorescence Microscopy section.

Tensile testing

All fibers were tested at room temperature and 25–30% RH approximately two weeks after spinning. During this interim, they were stored in a dry cabinet (Dry Keeper SUNPLATEC) at <20% RH. Every single fiber was mounted on a paper frame with a 1 × 1 cm open square window, providing an effective gauge length of ~1 cm. Fiber diameters were measured at five randomly selected points using light microscopy (Axioscope 5/7 KMAT, Zeiss), and the values were averaged according to previously described procedures. Tensile tests were performed using an Instron Single Column 5943 (Instron) at a strain rate of 6 mm/min. Engineering stress was calculated under the assumption of a circular cross-section. From the resulting engineering stress–strain curves, Young's modulus was determined by linear regression over the initial elastic region (up to 2% strain). Strength was taken as the stress at fracture, and Toughness modulus was calculated as the area under the curve. A minimum of ten fibers per sample type were tested. Statistical analysis was performed using a single one-tailed pairwise ANOVA with Prism (version 10.6.1, GraphPad).

Data availability

The data that support the findings of this study are available from the corresponding author upon reasonable request.

Received: 19 September 2025; Accepted: 13 January 2026;
Published online: 20 January 2026

References

1. Gosline, J. M., Guerette, P. A., Ortlepp, C. S. & Savage, K. N. The mechanical design of spider silks: from fibroin sequence to mechanical function. *J. Exp. Biol.* **202**, 3295–3303 (1999).
2. Braxton, T., Holland, C. & Greco, G. The circular argument behind spider and silkworm silk mechanical properties. *Mater. Des.* **260**, 115224 (2025).
3. Breslauer, D. N. Current Progress on Scale-Up and Commercialization of Microbially-Produced Silk. *Adv. Funct. Mater.* https://doi.org/10.1002/adfm.202408386 (2024).
4. Guessous, G., Blake, L., Bui, A., Woo, Y. & Manzanarez, G. Disentangling the web: an interdisciplinary review on the potential and feasibility of spider silk bioproduction. *Acs Biomater. Sci. Eng.* **10**, 5412–5438 (2024).
5. Schmuck, B. et al. Strategies for making high-performance artificial spider silk fibers. *Adv. Funct. Mater.* **34**, 2305040 (2024).
6. Schiller, T. & Scheibel, T. Bioinspired and biomimetic protein-based fibers and their applications. *Commun. Mater.* **5**, 56 (2024).
7. Andersson, M. et al. Biomimetic spinning of artificial spider silk from a chimeric minispidroin. *Nat. Chem. Biol.* **13**, 262–264 (2017).
8. Schmuck, B. et al. High-yield production of a super-soluble miniature spidroin for biomimetic high-performance materials. *Mater. Today* **50**, 16–23 (2021).
9. Pasupuleti, R. et al. Site-specific functionalization of recombinant spider silk using enzymatic sortase coupling. *Acs Omega* **10**, 5943–5952 (2025).
10. Fan, R. X. et al. Sustainable spinning of artificial spider silk fibers with excellent toughness and inherent potential for functionalization. *Adv. Funct. Mater.* **35**, https://doi.org/10.1002/adfm.202410415 (2025).
11. Bowen, C. H. et al. Recombinant spidroins fully replicate primary mechanical properties of natural spider silk. *Biomacromolecules* **19**, 3853–3860 (2018).
12. Li, J. Y. et al. Microbially synthesized polymeric amyloid fiber promotes β-nanocrystal formation and displays gigapascal tensile strength. *Acs Nano* **15**, 11843–11853 (2021).

13. Xia, X. X. et al. Native-sized recombinant spider silk protein produced in metabolically engineered results in a strong fiber. *Proc. Natl. Acad. Sci. USA* **107**, 14059–14063 (2010).
14. Nakamura, H. et al. Correlating mechanical properties and sequence motifs in artificial spider silk by targeted motif substitution. *Acs Biomater. Sci. Eng.* https://doi.org/10.1021/acsbiomaterials.4c01389 (2024).
15. Orlandi, V. T., Martegani, E., Giaroni, C., Baj, A. & Bolognese, F. Bacterial pigments: a colorful palette reservoir for biotechnological applications. *Biotechnol. Appl. Bioc* **69**, 981–1001 (2022).
16. Ziarani, G. M., Moradi, R., Lashgari, N. & Kruger, H. G. in *Metal-Free Synthetic Organic Dyes* (eds Ghodsi Mohammadi Ziarani, Razieh Moradi, Negar Lashgari, & Hendrik G. Kruger) 1–7 (Elsevier, 2018).
17. Islam, T., Repon, M. R., Islam, T., Sarwar, Z. & Rahman, M. M. Impact of textile dyes on health and ecosystem: a review of structure, causes, and potential solutions. *Environ. Sci. Pollut. R.* **30**, 9207–9242 (2023).
18. Raja, A. S. M., Arputharaj, A., Saxena, S. & Patil, P. G. in *Water in Textiles and Fashion* (ed Subramanian Senthilkannan Muthu) 155–173 (Woodhead Publishing, 2019).
19. Ammayappan, L., Jose, S. & Arputha Raj, A. in *Green Fashion: Volume 1* (eds Subramanian Senthilkannan Muthu & Miguel Angel Gardetti) 185–216 (Springer Singapore, 2016).
20. Lara, L., Cabral, I. & Cunha, J. Ecological approaches to textile dyeing: a review. *Sustainability-Basel* **14**, https://doi.org/10.3390/su14148353 (2022).
21. Fried, R., Oprea, I., Fleck, K. & Rudroff, F. Biogenic colourants in the textile industry - a promising and sustainable alternative to synthetic dyes. *Green. Chem.* **24**, 13–35 (2022).
22. Yang, D., Park, S. Y. & Lee, S. Y. Production of rainbow colorants by metabolically engineered. *Adv. Sci.* **8**, https://doi.org/10.1002/advs.202100743 (2021).
23. Liljeruhm, J. et al. Engineering a palette of eukaryotic chromoproteins for bacterial synthetic biology. *J. Biol. Eng.* **12**, https://doi.org/10.1186/s13036-018-0100-0 (2018).
24. Watkins, T., Moffitt, K., Speight, R. E. & Navone, L. Chromogenic fusion proteins as alternative textiles dyes. *Biotechnol. Bioeng.* **121**, 2820–2832 (2024).
25. Arndt, T. et al. Engineered spider silk proteins for biomimetic spinning of fibers with toughness equal to dragline silks. *Adv. Funct. Mater.* **32**, 2200986 (2022).
26. Schmuck, B. et al. Impact of physio-chemical spinning conditions on the mechanical properties of biomimetic spider silk fibers. *Commun. Mater.* **3**, 83 (2022).
27. Shaner, N. C. et al. Improved monomeric red, orange and yellow fluorescent proteins derived from Discosoma sp red fluorescent protein. *Nat. Biotechnol.* **22**, 1567–1572 (2004).
28. Edlund, A. M., Jones, J., Lewis, R. & Quinn, J. C. Economic feasibility and environmental impact of synthetic spider silk production from Escherichia coli. *N. Biotechnol.* **42**, 12–18 (2018).
29. Gao, Z. W. et al. Structural characterization of minor ampullate spidroin domains and their distinct roles in fibroin solubility and fiber formation. *Plos One* **8**, https://doi.org/10.1371/journal.pone.0056142 (2013).
30. Hagn, F. et al. A conserved spider silk domain acts as a molecular switch that controls fibre assembly. *Nature* **465**, 239–U131 (2010).
31. Greco, G., Schmuck, B., Jalali, S. K., Pugno, N. M. & Rising, A. Influence of experimental methods on the mechanical properties of silk fibers: a systematic literature review and future road map. *Biophys. Rev. (Melville)* **4**, 031301 (2023).
32. Greco, G., Mirbaha, H., Schmuck, B., Rising, A. & Pugno, N. M. Artificial and natural silk materials have high mechanical property variability regardless of sample size. *Sci Rep-Uk* **12**, https://doi.org/10.1038/s41598-022-07212-5 (2022).
33. Schmuck, B., Greco, G., Shilkova, O. & Rising, A. Effects of mini-spidroin repeat region on the mechanical properties of artificial spider silk fibers. *ACS Omega* **9**, 42423–42432 (2024).
34. Jansson, R., Courtin, C. M., Sandgren, M. & Hedhammar, M. Rational design of spider silk materials genetically fused with an enzyme. *Adv. Funct. Mater.* **25**, 5343–5352 (2015).
35. Humenik, M., Mohrand, M. & Scheibel, T. Self-assembly of spider silk-fusion proteins comprising enzymatic and fluorescence activity. *Bioconjug. Chem.* **29**, 898–904 (2018).
36. da Silva, A. J. et al. Non-conventional induction strategies for production of subunit swine erysipelas vaccine antigen in fed-batch cultures. *Springerplus* **2**, https://doi.org/10.1186/2193-1801-2-322 (2013).
37. Gasteiger, E. et al. in *The Proteomics Protocols Handbook* (Walker, J. M. ed) 571–607 (Humana Press, 2005).
38. Schneider, C. A., Rasband, W. S. & Eliceiri, K. W. NIH Image to ImageJ: 25 years of image analysis. *Nat. Methods* **9**, 671–675 (2012).
39. Greco, G. et al. Properties of biomimetic artificial spider silk fibers tuned by PostSpin Bath incubation. *Molecules* **25**, https://doi.org/10.3390/molecules25143248 (2020).
40. Jafari, M. J. et al. Force-induced structural changes in spider silk fibers introduced by ATR-FTIR spectroscopy. *Acs Appl. Polym. Mater.* **5**, 9433–9444 (2023).
41. Rana, M. S., Wang, X. Y. & Banerjee, A. An improved strategy for fluorescent tagging of membrane proteins for overexpression and purification in mammalian cells. *Biochemistry* **57**, 6741–6751 (2018).

Acknowledgements

This work was supported by grants from Olle Engkvist stiftelse (233-0334), Knut and Alice Wallenberg Foundation (2023.0331, WASP-DDLS2 2:035 and Wallenberg Launch Pad), FORMAS (2023-01313), and the Swedish Research Council (2024-02919) to A.R. B.S. was supported by FORMAS (2023-00871). G.G. was supported by the project "EPASS" under the HORIZON TMA MSCA Postdoctoral Fellowships - European Fellowships (project number 101103616). A special thank you to Anil Putri for assisting in protein purification.

Author contributions

A.R. was the principal investigator of this study and conceived the idea. T.B.P. and B.S. expressed and purified the proteins. B.S. conducted the spinning experiments. G.G. performed the tensile tests, calculated the mechanical properties, and analyzed the data. S.S. and B.G. performed microscopy and evaluated the data. E.K. conducted FTIR measurements. A.L. and M.L. performed MS and MP experiments. All authors discussed the results. The first draft of the manuscript was written by T.B.P., B.S., and A.R., and edited by all authors.

Funding

Open access funding provided by Swedish University of Agricultural Sciences.

Competing interests

The authors declare no competing interests.

Additional information

Supplementary information The online version contains supplementary material available at https://doi.org/10.1038/s43246-026-01079-z.

Correspondence and requests for materials should be addressed to Anna Rising.

Peer review information *Communications Materials* thanks Mattheos Koffas and the other, anonymous, reviewer for their contribution to the peer review of this work. A peer review file is available.